

# Molecular Dynamics (MD) Simulation of Multi-pass Nanometric Machining – The Effect of Machining Conditions

Akinjide Olufemi Oluwajobi<sup>\*a</sup> and Xun Chen<sup>b</sup>

<sup>a</sup>Department of Mechanical Engineering, Faculty of Technology, Obafemi Awolowo University, Ile-Ife, 220005, Nigeria;

<sup>b</sup>General Engineering Research Institute, Liverpool John Moores University, Liverpool, L3 3AF, UK

**Abstract:** Understanding material behaviour during nanoscale machining is critical for improving machining efficiency. This paper investigates the benefits of using Molecular Dynamics (MD) simulation in studying the effects of machining parameters in nanometric machining of copper workpiece with a diamond tool. The material behaviour under multi cutting pass conditions was examined. The copper-copper interactions were modelled by the EAM potential and the copper-diamond interactions were modelled by the Morse potential. The diamond tool was modelled as a deformable body and the Tersoff potential was applied for the carbon-carbon interactions. It was observed that the average tangential and normal components of the cutting forces increase with increase in depth of cut and they reduced in consecutive cutting passes for each depth of cut. The ratios of the tangential to the normal force components decreases as the depth of cut increases, but remain constant after the depth of cut 1.5nm. The magnitudes of the cutting forces decrease from pass 1 to pass 2, but they are identical for both pass 2 and pass 3. The least resistance to cutting was observed at 2.0nm, which may indicate the existence of a critical depth of cut in nanomachining, for tool wear reduction. After the first pass, the average tangential and normal components of the cutting forces increase with increase in the feed. Also, there is always an increase in friction from pass 1 to pass 2. In multipass processes, the arrangement should be effected with minimum overlap in the runs, for efficient machining.



**Keywords:** : Multiple Pass, Molecular Dynamics, Nano Surfaces, Depth of Cut, Feed Rate, Materials Behaviour, Nanometric Machining

## 1. INTRODUCTION

The material removal in precision machining is often at the nanometre scale with stringent form and surface finish accuracy. At this length scale, machining phenomena take place in a small limited region of tool – workpiece interface, which often contains a few atoms or layers of atoms. At present, it is very difficult to observe the diverse microscopic physical phenomena through experiments at the nanoscale [1]. The interface at this level may not be considered as a continuous media or homogeneous as assumed by continuum mechanics, so the analysis should be based on discrete atoms whose interactions are governed by appropriate interatomic potentials. The use of Molecular Dynamics (MD) simulation has proved to be an effective tool for the investigation of machining processes at the nanometre scale [2, 3, 4]. The method gives higher resolution of the cutting process than what is possible by continuum mechanics on that length scale [5].

The MD method was initiated in the late 1950s at Lawrence Radiation Laboratory in the US by Alder and Wainwright in the study of statistical mechanics [6]. Since then, the use of the simulation method has extended from Physics to Materials Science and now to Mechanical Engineering. Rentsch and Inasaki [3] modelled a copper workpiece and a diamond tool using the Lennard-Jones potential for the copper atom interactions. They observed a build-up phenomenon after 25000 time steps, while keeping the tool rigid. Komanduri et al [4] used copper workpiece and an infinitely hard tungsten tool for their simulation. They used Morse potentials and a cutting speed of 500m/s. They observed increase in the cutting forces, the force ratio, the specific energy and the sub-surface deformation with increase in the negative rake of the tool.

Many current MD simulation studies on nanometric cutting have been focused on single cutting pass or simple line-type groove. In extending the single pass studies, Zhang et al [7] modelled folder- line grooves for Atomic Force Microscopy (AFM) -based nanometric cutting process of copper with diamond tool. The investigation focused on the effect of groove type (line and folder line) and geometry

<sup>\*</sup>Address correspondence to this author at the Department of Mechanical Engineering, Faculty of Technology, Obafemi Awolowo University, P.M. B. 13: 220005, Ile-Ife, Nigeria; Tel: +234-705811389; E-mail: [aogunjob@oauife.edu.ng](mailto:aogunjob@oauife.edu.ng)

(folder angle; 0°, 30°, 45°, 60° and 90°) on the groove fabrication process. They employed the Embedded Atom Method (EAM) potential for the copper-copper interactions and the Morse potential for the copper-diamond interactions. They treated the diamond tool as a rigid tool and concluded that the normal, lateral and the resultant forces were almost symmetric with respect to the critical folder angle of 45°. Shi et al [8] investigated the multi-groove simulation of single-point turning of copper with diamond tool. They used a two-groove cutting procedure and modelled the copper-copper and the copper-diamond interactions by using the Morse potential. They also treated the tool as a rigid body and observed that the tool's forces increase with increase in feed rate and depth of cut. The MD simulation of multi-path processes in the cutting of copper workpiece by a diamond tool was investigated by Chen et al [9]. They observed that the reciprocating cutting force and the prior cutting force from the two pass operation decreases as the cutting depth decreases. The affected zone from the second feed cutting process was larger than that from the prior cutting process. Dislocation activities were reported to occur during the cutting process, and it was noted that dislocation nucleation was near the free surface and it propagated in the surface and downward in the workpiece. The surface roughness obtained after the machining and the scratched groove shape, was found to be related to the offset distance of the tool. The copper-copper interactions were modelled by the EAM potential, the copper-diamond interactions were modelled by the Morse potential and the tool was treated as rigid.

Recently, Tong et al [10] and Luo et al [11] studied the mechanism of machining nanostructures by using single tip and multi-tip diamond tools. The MD simulations were conducted on diamond tools and copper workpiece. The copper-copper interactions were modelled by the EAM potential and the tool-workpiece interaction was modelled by the Morse potential. However, the diamond tools were treated as deformable and they were modelled by the Tersoff potential. In the study, the single tip tool was used with two passes and the multi-tip tool was used with a single pass. It was observed that, when the cutting stage was steady, the process was characterized by a strong localization of dislocation movement and the dynamic equilibrium of the chip-tool contact area. The multi-tip tool was found to be more suitable than the single tip tool, for scale-up fabrication of nanostructures. Also, they established that the tool-tip angle of the multi-tip tool has a significant influence on the quality of the machined nanostructures. In practice, many machining processes involve the use of multiple passes to create a new surface and the diamond tool is actually deformable [12, 13]. In this study, the effect of depth of cut and scribing feed on the simulation of multi-pass cutting, was investigated in the surface creation process, as in single point diamond turning.

## 2. THE MD METHODOLOGY

MD is a computer simulation technique by which the atomic trajectories of a set of  $N$  particles are generated by the numerical integration of Newton's equation of motion [14]. It is a deterministic method, which implies that the state of the system at any future time can be predicted from its

current state [15]. Paradoxically, the method is also based on statistical mechanics and a probabilistic approach is used to obtain a set of configurations distributed according to some statistical ensemble [16]. The MD simulation consists of the numerical step-by-step solution of the classical equations of motion based on Newton's second law (Eq. 1). For a set of  $N$  particles or atoms,

$$F_i = m_i a_i \quad (1)$$

Where  $m_i$  is the mass of atom I,  $a_i = \frac{d^2 r_i}{dt^2}$  is the acceleration of the atom I and  $F_i$  is the resultant force acting on atom i. These forces should be balanced by the potential energy between atoms, which are usually presented as the gradient of a potential energy function.

Many interatomic potentials have been applied in the MD simulation of nanometric machining. The most commonly used ones are the Lennard-Jones (LJ), Morse and the Embedded Atom Method (EAM) for the modelling of the workpiece. It is very important to select adequate interatomic potentials for the modelling of materials used in the MD simulations [17], but many researchers sometimes use various interatomic potentials for nanometric machining simulation without justifications. In previous studies, it has been established that the EAM potential is very suitable for the Cu-Cu interactions [17, 18, 19]; for the Cu-C interactions; the Morse potential has been used successfully, as there are no dedicated potentials for the interactions [16]; and for the C-C interactions in the tool, the Tersoff potential have been used [10,11,12,13].

### 2.1 Potential functions and modelling parameters for the simulation

*Embedded-Atom Method Potential (EAM)* (Eq. 2) [20] (For the Cu-Cu interactions)

$$E_{tot} = \sum_i G_i(\rho_{h,i}) + \frac{1}{2} \sum_{i,j} V_{ij}(r_{ij}) \quad (2)$$

Where  $\rho_{h,i}$  is the total electron density at atom i due to the rest of the atoms in the system.

$G_i$  is the embedding energy for placing an atom into the electron density,  $V_{i,j}$  is the short range pair interaction representing the core-core repulsion,  $r_{ij}$  is the separation of atoms i and j

*Morse Potential* (Eq. 3) [21] (For the Cu-C interactions)

$$V_{ij} = D\{\exp[-2\alpha(r_{ij} - r_e)] - 2\exp[-\alpha(r_{ij} - r_e)]\} \quad (3)$$

Where  $r_{ij}$  and  $r_e$  are instantaneous and equilibrium distances between atoms  $i$  and  $j$  respectively

$\alpha$  and  $D$  are constants determined on the basis of the physical properties of the material

The parameters used in the simulations are below, [22];

$$D = 0.087 \text{ eV}, \alpha = 0.17 (\text{nm})^{-1}, r_e = 0.22 \text{ nm}$$

The cut-off distance chosen was 6.4 Angstroms (that is, the interactions between atoms separated by more than this distance are neglected).

*Tersoff Potential* (Eq. 4) [23] (For the C-C interactions)

$$E = \sum_i E_i = \frac{1}{2} \sum_i \sum_{j \neq i} V_{ij} \quad (4)$$

and,

$$V_{ij} = f_C(r_{ij})[a_{ij}f_R(r_{ij}) + b_{ij}f_A(r_{ij})]$$

where

$$f_R(r) = A \exp(-\lambda_1 r),$$

$$f_A(r) = -B \exp(-\lambda_2 r),$$

$$f_C(r) = \begin{cases} 1, & r < R - D \\ \frac{1}{2} - \frac{1}{2} \sin \left[ \frac{\pi}{2} (r - R) / D \right], & R - D < r < R + D \\ 0, & r > R + D \end{cases}$$

$$b_{ij} = (1 + \beta^n \zeta_{ij}^n)^{-1/2n},$$

$$\zeta_{ij} = \sum_{k(\neq i, j)} f_C(r_{ik}) g(\theta_{ijk}) \exp[\lambda_3^3 (r_{ij} - r_{ik})^3],$$

$$g(\theta) = 1 + \frac{p^2}{q^2} - \frac{p^2}{[q^2 + (h - \cos \theta)^2]},$$

$$a_{ij} = (1 + \alpha^n \eta_{ij}^n)^{-1/2n},$$

$$\eta_{ij} = \sum_{k(\neq i, j)} f_C(r_{ik}) \exp[\lambda_3^3 (r_{ij} - r_{ik})^3]$$

Where  $R$  and  $D$  are cut-off parameters;  $A, B, \lambda_1, \lambda_2, \lambda_3, \alpha, \beta, n, p, q, h$  are fitting parameters of the Tersoff potential. The simulation parameters used for carbon, are given in table 1.

**Table 1. Constants for Tersoff potential** [23, 24, 25, 26]

Parameters	Carbon
A(eV)	$1.3936 \times 10^3$
B(eV)	$3.467 \times 10^2$
$\lambda_1 (\text{nm}^{-1})$	34.879
$\lambda_2 (\text{nm}^{-1})$	22.119
$\alpha$	0.0
$\beta$	$1.5724 \times 10^{-7}$
n	$7.2751 \times 10^{-1}$
p	$3.8049 \times 10^4$
q	4.384
h	$-5.7058 \times 10^{-1}$
$\lambda_3 (\text{nm}^{-1})$	22.119
R (nm)	0.18
D(nm)	0.02

## 2.2. MD simulation for nano-machining

In order to carry out a MD simulation study, an adequate simulation environment has to be set up. The configuration model has a total of 54232 atoms. The workpiece consists of 43240 copper atoms with the FCC lattice. It includes 3 kinds of atoms namely; boundary atoms, thermostat atoms and Newtonian atoms (See Figure 1). The cutting tool consists of 10992 carbon atoms with diamond lattice structure. Fig. 2 shows a diagram of the machined grooves with passes 1, 2 and 3. The scribing feed is shown in the figure and this was varied from (0.5 to 1.5nm) in the simulation.

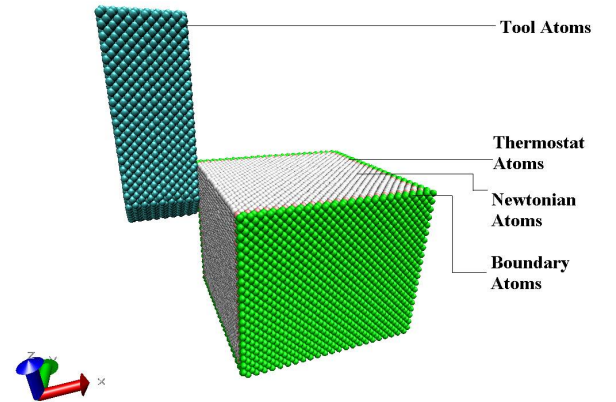


**Figure 1: The MD Simulation Model**

The simulation conditions applied in this study are the following, viz; Bulk temperature is 293K, the cutting direction is along the x-axis, the cutting speed is 150m/s, the time step is 0.3fs and the simulation run is 150000 steps.

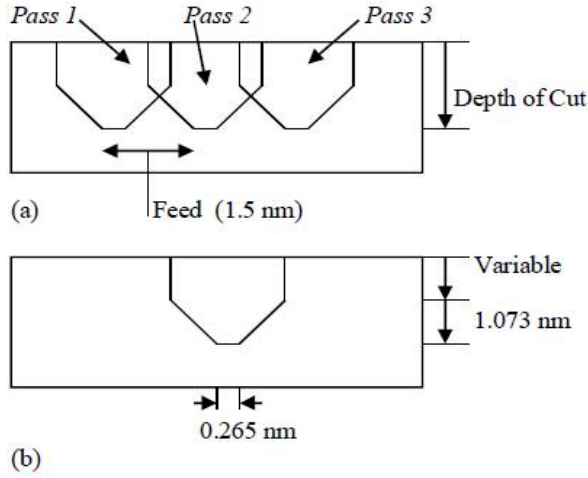


**Figure 2: Cross Section of the Machined Grooves with Pass 1-3 (direction of cut is perpendicular to the paper face)**

The cutting tool has a trapezoidal end shape for convenience; it could have been rounded at the edges, but the effect on the simulations should be insignificant. The positions of the boundary atoms are kept fixed to reduce edge effects. The thermostat atoms conduct the heat generated during the cutting process out of the cutting region. This is achieved by the velocity scaling of the thermostat atoms, (with the conversion between the kinetic energy (KE) and temperature as in (Eq. 5) [27, 28]);

$$\sum_i \frac{1}{2} m_i v_i^2 = \frac{3}{2} N k_B T_i \quad (5)$$

Where  $m_i$  is the mass of the  $i$ th atom,  $v_i$  is the resultant velocity of the  $i$ th atom,  $N$  is the number of the thermostat atoms,  $T_i$  is the temperature of the  $i$ th atom and  $k_B$  is the Boltzmann constant ( $1.3806504 \times 10^{-23} \text{ JK}^{-1}$ )

Whenever the temperature of the thermostat atoms exceeds the preset bulk temperature of 293K, their velocities are scaled by using (Eq. 6) [29, 30];

$$v_{i,new} = v_i \sqrt{\frac{T_{desired}}{T_{current}}} \quad (6)$$

Where  $T_{current}$  is the current temperature that is calculated from the KE and the  $T_{desired}$  is the desired temperature which is preset. The Newtonian atoms obey the Newton's equation of motion. The depths of cut used in the study are 0.5nm, 1.0nm, 1.5nm, 2nm, 2.5nm and 3 nm. For the feed rate; the following were used namely; 0.5nm, 0.75nm, 1.0nm, 1.25nm and 1.5nm. The LAMMPS MD software [31]

was used for the simulations and the VMD software [32] was used for the visualization of the results.

### 3. RESULTS AND DISCUSSION

Table 2 shows the results of the simulations for depths of cut of 0.5nm, 1.5nm, 2.5nm, and for the 3 passes. From Table 2; the simulations show the material removal mechanisms at the different depths of cut. For the first pass, the diamond tool approaches the workpiece at the onset of the simulation, and as the tool touches the workpiece, there is momentarily adhesion of the tool atoms and the workpiece atoms. As this is overcome, the tool moves through the workpiece, by ploughing and cutting, depending on the depth of cut. At the cutting depth of 0.5nm, only ploughing occurs and at 1.5nm and 2.5nm, chip formation takes place. Both phenomena of ploughing and cutting are associated with plastic deformation and dislocation activities. The chip formation has been well documented to be associated with dislocations initiation and propagation on the (111) crystal slip planes [10][33]. It can be observed that the amount or volume of atoms removed from the workpiece increases as the depth of cut increases, which is logical, because as the depth increases, the tool-chip contact area increases, and so there is more volume of material atoms to be removed. Subsequently, for the second and third passes, less volume of atoms are ploughed and cut through, because of less portion of the workpiece engaged with the tool. Also, more complex interplay of dislocation movements are evident.

Figures 3-5 show the cutting forces for the corresponding simulations, for passes 1 and 2. The magnitudes of the cutting forces decrease from pass 1 to pass 2, but they are identical for both pass 2 and pass 3 (though Figures for pass 3 are not shown). The resistance to overcome in the first pass during cutting is more than that for passes 2 and 3. This is similar to the results obtained by Chen et al [9], where the prior cutting force decreased from the two pass operations, even though their own two pass runs were independent. On the other hand, the cutting forces increase as the depth of cut increases. The negative forces observed for  $F_z$  is depicted to show that the direction is opposite to the positive axis.

Cutting forces were obtained for the following parameters; different depths of cut (0.5 ~ 2.5nm), feed = 1.5nm, cutting speed = 150m/s and rake angle =  $0^\circ$ .  $F_x$  is the tangential force component (cutting force),  $F_z$  is the normal/perpendicular force and  $F_y$  is the lateral force. Figures 6-9 show the variation of the forces with depth of cut, for the passes. For the different passes,  $F_x$  increases with increase in depth of cut and  $F_x$  is larger in pass 1 than in passes 2 and 3.

The force,  $F_x$  is higher for cutting than for ploughing and the sudden change in the cutting force is caused by the repulsion of the tool and the workpiece, after the initial adhesion.  $F_y$  increases in pass 1 and decreases in pass 2 and 3; with increase in the depth of cut. The variation is quite small as shown in Figure 7, as  $F_y$  is supposed to be zero theoretically.  $F_z$ , as shown in Figure 8, is similar also to  $F_x$ . It increases in magnitude with increase in depth of cut. It can also be seen that the normal force component,  $F_z$  is relatively smaller for small depths of cut, 0.5nm and 1.5nm than for higher depths

of cut. This is so because of the shape of the diamond tool, which makes less contact area for smaller depth of cut. The average tangential and the normal force components decrease with the consecutive passes. Figure 9 shows the variation of the cutting forces with depth of cut for pass 3. It can be seen that the magnitude of the tangential force component is higher than that of the normal force component.

**Table 2. Simulations for Different Depths of Cut (0.5 ~ 2.5nm), Feed = 1.5nm, Cutting Speed = 150m/s, Rake Angle = 0°**

**Figure 3: Cutting Forces for Depth of Cut – 0.5nm (a – Pass 1; and b- Pass 2)**

**Figure 4: Cutting Forces for Depth of Cut – 1.5nm (a – Pass 1; and b- Pass 2)**

**Figure 5: Cutting Forces for Depth of Cut – 2.5nm (a – Pass 1; and b- Pass 2)**

**Table 3. Force Ratios for Different Depth of Cut (0.5~3.0nm)**

**Figure 6: Variation of  $F_x$  with Depth of Cut**

**Figure 7: Variation of  $F_y$  with Depth of Cut**

**Figure 8: Variation of  $F_z$  with Depth of Cut**

**Figure 9: Variation of  $F_x$ ,  $F_y$  and  $F_z$  in Pass 3 with Depth of Cut**

Table 3 shows the force ratios for depth of cut (0.5nm~3.0nm) for the three passes, which is a measure of friction. It is a measure of the resistance that the tool experiences when ploughing and when cutting through the workpiece. It is estimated as in macro machining, to be the ratio of the tangential force to the normal force ( $F_x/F_z$ ). For the depth of cut (0.5), during ploughing, the normal forces are very low compared to the tangential forces and consequently the force ratio is quite high. It is similar for all the passes. It is reduced during cutting, as the normal forces increases. It can be seen that the ratio decreases as the depth of cut increases up to around 1.5nm and then remains fairly constant. This might also be due to the tool geometry. There is always a reduction in the friction between pass 1 and pass 2, for all the depths of cut. This may be because, after the first pass, and the subsequent material removal, there would be less tool-chip contact area during the second pass, which could lead to the less resistance. The frictions due to the third pass appear to be higher than the other passes, except for the depth of cut of 0.5nm (that is during ploughing). This seems unclear except for the possible interactions with the boundary atoms. The least resistance to cutting is observed at the depth of cut of 2.0nm, which may indicate the existence of a critical depth of cut that would reduce wear on the tool, during the machining process.

Further simulations and cutting forces were obtained for the following parameters; feed (0.5 ~ 1.5nm),

depth of cut = 2nm, cutting speed = 150m/s and rake angle = 0°, and are shown in Table 4, Figures 10-12. (Note: a cross feed of 1.5nm was used for the depth of cut variation simulations in Table 2). Figures 10 -12 show the cutting forces for passes 1 and 2, for cross feed 0.5nm, 1.0nm and 1.5nm. The magnitudes of the cutting forces decrease from pass 1 to pass 2, but they are identical for both pass 2 and pass 3. As noted earlier, the resistance to overcome in the first pass during cutting is more than that for passes 2 and 3.

Figures 13-14 show the variation of  $F_x$  with feed, for the different passes. It can be observed that,  $F_x$  fairly remains constant, as the scenario is similar for all the initial ploughing/cutting process for pass 1, for all feeds. This repeats for the absolute values of normal force. Table 5 shows the force ratios for feed (0.5nm~1.5nm) for the three passes. As can be observed, the larger the cross feed value, the less friction the tool encounters during the nanomachining. The tool has a width of around 1.5nm, and it may mean that when carrying out multipass processes, the passes should be achieved with minimum overlap in the runs. Also, there is always an increase in friction between pass 1 and pass 2, for all the cross feed, even though the values are close for pass 2 and pass 3.

**Table 4. Simulations for Different Feed (0.5 ~ 1.5nm), Depth of Cut = 2nm, Cutting Speed = 150m/s, Rake Angle = 0°**

**Figure 10: Cutting Forces for Feed – 0.5nm (a - Pass 1 and b – Pass 2)**

**Figure 11: Cutting Forces for Feed – 1.0nm (a - Pass 1 and b – Pass 2)**

**Figure 12: Cutting Forces for Feed – 1.5nm (a - Pass 1 and b – Pass 2)**

**Figure 13: Variation of  $F_x$  with Passes 1~3**

**Figure 14: Variation of  $F_z$  with Passes 1~3**

**Table 5: Force Ratios for Feed (0.5~1.5nm)**

## CONCLUSION

The MD simulation of the multiple pass nanometric machining process has been clearly demonstrated. It has been observed that the average tangential and normal components of the cutting forces increase with increase in depth of cut and they reduced in consecutive cutting passes for each depth of cut. The ratios of the tangential to the normal force components decreases as the depth of cut increases, but remain constant after the depth of cut 1.5nm. The magnitudes of the cutting forces decrease from pass 1 to pass 2, but they are identical for both pass 2 and pass 3. The least resistance to cutting was observed at 2.0nm, which may indicate the existence of a critical depth of cut for tool wear reduction. With the variation of the cross feed, after the first pass, the average tangential and normal components of the cutting forces increase with increase in the feed. Also, there is always an increase in friction from pass 1 to pass 2. When

carrying out multipass processes, the arrangement should be effected with minimum overlap in the runs, for efficient machining.

## REFERENCES

- [1] Rentsch, R. Nanoscale cutting, In: *Nano and Micromachining*; Davim, J. P.; Jackson, M. J. Eds.; Wiley-ISTE, **2008**; pp.1-24.
- [2] Shimada, S.; Ikawa, N.; Ohmori, G.; Tanaka, H.; Uchikoshi, U. Molecular dynamics analysis as compared with experimental results of micromachining, *Annals of the CIRP*, **1992**, 41(1), 117-120.
- [3] Rentsch, R.; Inasaki, I. Molecular dynamics simulation for abrasive processes, *Annals of the CIRP*, **1994**, 43(1), 327-330.
- [4] Komanduri, R.; Chandrasekaran, N.; Raff, L. M. Some aspects of machining with negative-rake tools simulating grinding: A molecular dynamics simulation approach, *Philosophical Magazine B*, **1999**, 79(7), 955-968.
- [5] Komanduri, R.; Raff, L. M. A review on the molecular dynamics simulation of machining at the atomic scale, *Proceedings of the Institution of Mechanical Engineers, B*, **2001**, 215, 1639-1672.
- [6] Alder, B. J.; Wainwright, T.E. Studies in molecular dynamics. I. General method *Journal of Chemical Physics*, **1959**, 31, 459-466.
- [7] Zhang, J.T.; Sun, T.; Yan, Y.; Liang, Y.; Dong, S. Molecular dynamics study of groove fabrication process using AFM-based nanometric cutting technique, *Applied Physics A (Materials Science and Processing)*, **2009**, 94(3), 593-600.
- [8] Shi, J.; Shi, Y.; Liu, C. R. Evaluation of a three-dimensional single-point turning at atomistic level by a molecular dynamics simulation, *International Journal of Advanced Manufacturing Technology*, **2011**, 54(1-4), 161-171.
- [9] Chen, J.; Liang, Y.; Chen, M.; Wang, L. Multi-path nanometric cutting of molecular dynamics simulation, *Journal of Computational and Theoretical Nanoscience*, **2012**, 9, 1303-1308.
- [10] Tong, Z.; Liang, Y.; Jiang, X.; Luo, X. An investigation on the mechanism of machining nanostructures when using single tip and multi-tip diamond tools, *Applied Surface Science*, **2014**, 290, 458-465.
- [11] Luo, X.; Tong, Z.; Liang, Y. Investigation of shape transferability of nanoscale multi-tip diamond tools in the diamond turning of nanostructures, *Applied Surface Science*, **2014**, 321, 495-502.
- [12] Oluwajobi, A. O.; Chen, X. Multi-pass nanometric machining simulation using the molecular dynamics (MD), *Key Engineering Materials*, **2012**, 496, 241-246.
- [13] Oluwajobi, A.O.; Chen, X. In: *The Effect of Depth of Cut on the Molecular Dynamics (MD) Simulation of Multi-pass Nanometric Machining*, In: Proceedings of the 17<sup>th</sup> International Conference on Automation & Computing, **2011**, pp. 40-45.
- [14] Li, J. Basic Molecular Dynamics in Yip S (Ed): *Handbook of Materials Modelling Springer* **2005**; pp. 565-588.
- [15] Leach, A. *Molecular Modelling: Principles and Applications*: Prentice Hall, **2001**.
- [16] Ercolessi, F. A Molecular Dynamics Primer *Spring College in Computational Physics ICTP Trieste* <http://www.fisica.uniud.it/~ercolessi/md/md/> (Accessed in March 31, **2011**).
- [17] Oluwajobi, A.; Chen, X. The effect of interatomic potentials in the molecular dynamics simulation of nanometric machining, *International Journal of Automation and Computing*, **2011**, 326-332.
- [18] Oluwajobi, A. O.; Chen, X. The Fundamentals of Modelling Abrasive Machining using Molecular Dynamics, *International Journal of Abrasive Technology*, **2010**, 3(4), 354-381.
- [19] Pei, Q. X.; Lu, C.; Fang, F. Z.; Wu, H. Nanometric cutting of copper: A molecular dynamics study *Comp.Mat. Sci*, **2006**, 37, 434-441.
- [20] Foiles, S. M. Application of the embedded atom method to liquid transition metals, *Physical Review B*, **1985**, 32(6), 3409-3415.
- [21] Morse, P. M. Diatomic molecules according to wave mechanics II vibrational levels, *Physical Review*, **1929**, 34, 57-64.
- [22] Hwang, H. J.; Kwon, O-K.; Kang, J. W. Copper nanocluster diffusion in carbon nanotube, *Solid St. Comm.*, **2004**, 129, 687-690.
- [23] Tersoff, J. New empirical approach for the structure and energy of covalent systems, *Physical Review B*, **1988**, 37(12), 6991-7000.
- [24] Tersoff, J. Empirical interatomic potential for silicon with improved elastic properties, *Physical Review B*, **1988**, 38(14), 9902-9905.
- [25] Raffi-Tabar, H.; Mansoori, G. A. Interatomic Potential Models for Nanostructures, In: *Encyclopedia of Nanoscience and Nanotechnology* Nalwa, H.S. ed.; American Scientific Publishers, **2003**, X, pp.1-17.
- [26] Saito, Y.; Sasaki, N.; Moriya, H.; Kagatsume, A.; Noro, S. Parameter optimization of Tersoff interatomic potentials using genetic algorithms, *JSME International Series A*, **2001**, 44(2), 207-213.
- [27] Cai, M.; Li, X.; Rahman, M. Molecular dynamics modelling and simulation of nanoscale ductile cutting of silicon, *International Journal of Computer Applications in Technology*, **2007**, 28(1), 2-8.
- [28] Guo, Y.; Liang, Y.; Chen, M.; Bai, Q.; Lu, L. Molecular dynamics simulations of thermal effects in nanometric cutting process, *Science China Technological Sciences*, **2010**, 53(3), 870-874.
- [29] Cheong, W. C. D.; Zhang, L.; Tanaka, H. Some essentials of simulating nano-surface processes using the molecular dynamics method, *Key Engineering Materials*, **2001**, 196, 31-42.
- [30] Lin, Z -C.; Chen, Z -D.; Huang, J -C. Establishment of a cutting force model and study of the stress-strain distribution in nano-scale copper

material orthogonal cutting, *International Journal of Advanced Manufacturing Technology*, **2007**, 33(5-6), 425-435.

[31] Plimpton, S.J. Fast parallel algorithms for short-range molecular dynamics, *Journal Comp. Phys.*, **1995**, 117, 1- 19.

[32] Visual Molecular Dynamics (VMD), <http://www.ks.uiuc.edu/Research/vmd/> (Accessed Dec 31, **2010**).

[33] Chen, M.; Xiao.G.; Lo, L.; Wu, C. Mechanism of chip-formation in nanometric cutting of single-

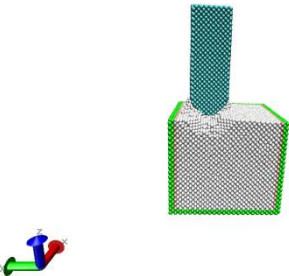
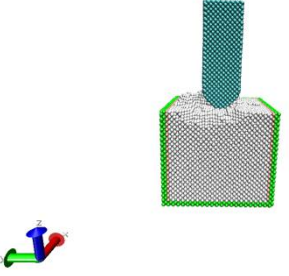
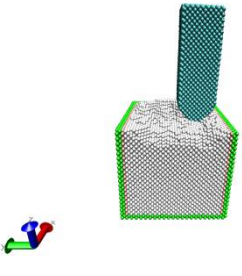
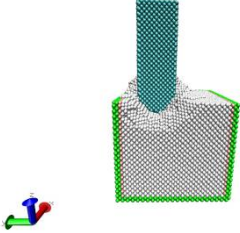
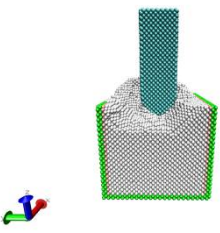
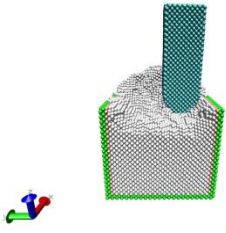
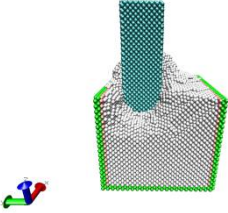
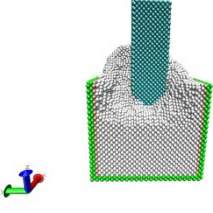
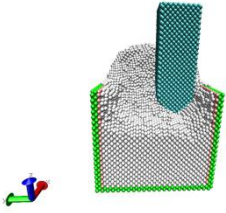
copper by molecular dynamics, *Journal of Computational and Theoretical Nanoscience*, **2012**, 9(1), 110-116.

Received: March 20, 2014

Revised: April 16, 2014

Accepted: April 20, 2014

**Table 2. Simulations for Different Depths of Cut (0.5 ~ 2.5nm), Feed = 1.5nm, Cutting Speed = 150m/s, Rake Angle = 0°**

Depth of Cut (nm)	Pass 1	Pass 2	Pass 3
0.5			
1.5			
2.5			



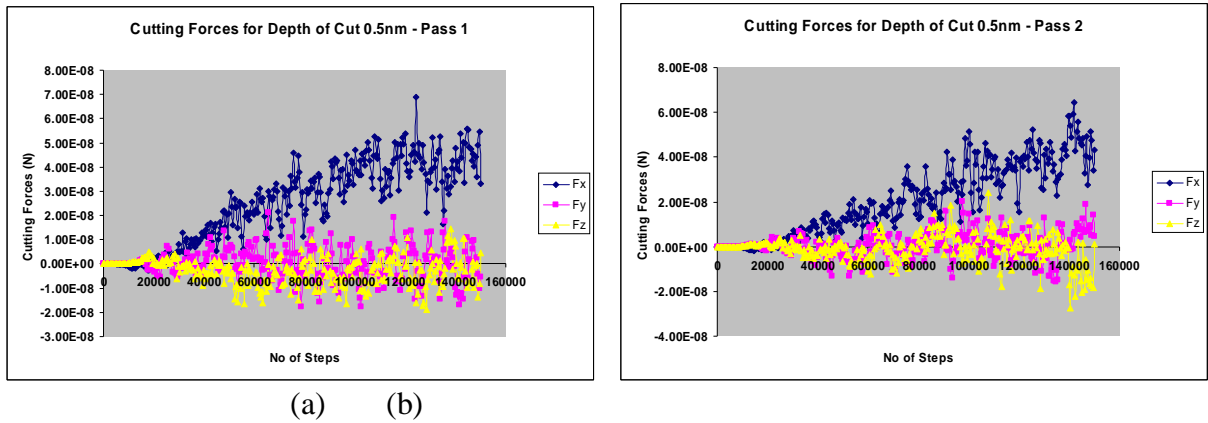


Figure 3: Cutting Forces for Depth of Cut – 0.5nm (a –Pass 1; and b- Pass 2)

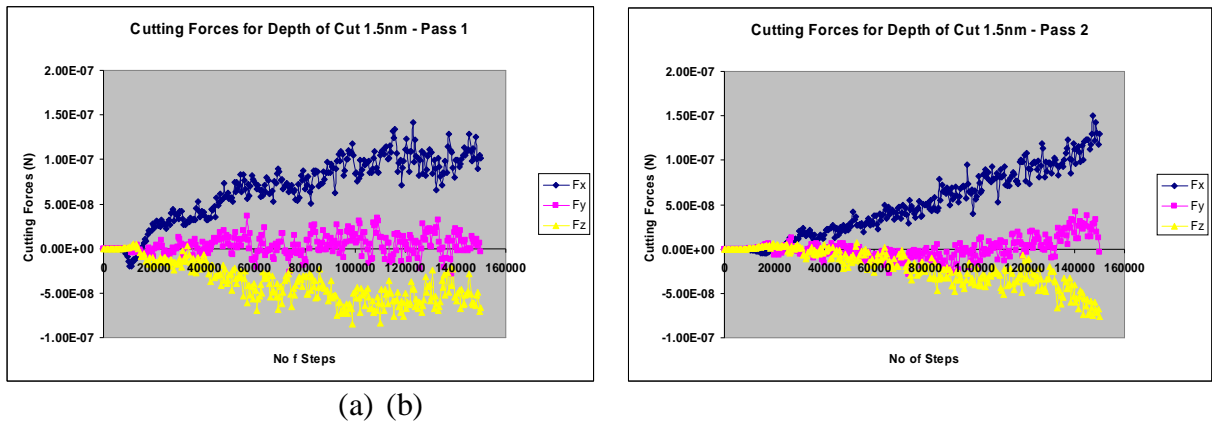
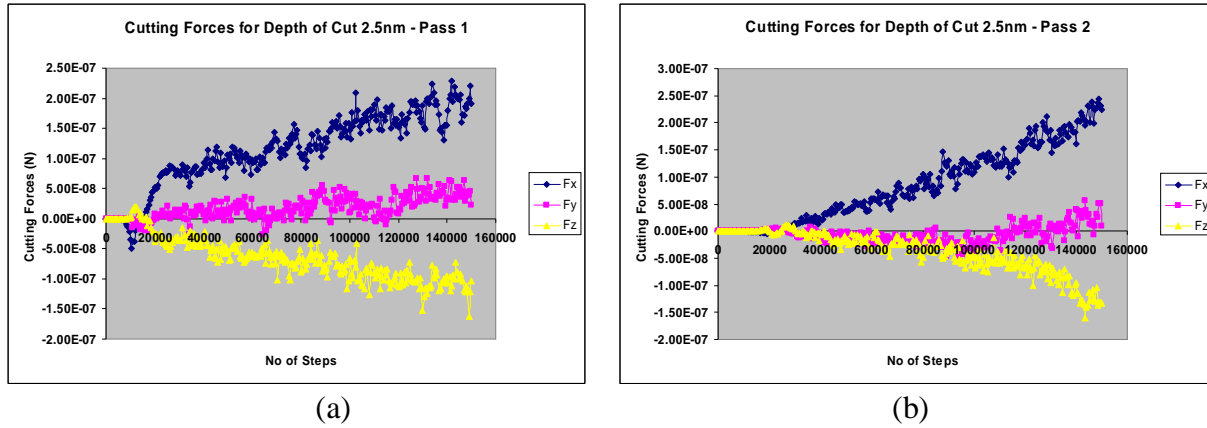


Figure 4: Cutting Forces for Depth of Cut – 1.5nm (a –Pass 1; and b- Pass 2)





**Figure 5: Cutting Forces for Depth of Cut – 2.5nm (a –Pass 1; and b- Pass 2)**

**Table 3. Force Ratios for Different Depth of Cut (0.5~3.0nm)**

Depth of Cut (nm)	$F_x/F_z$ Pass 1	$F_x/F_z$ Pass 2	$F_x/F_z$ Pass 3
0.5	8.80451	7.327466	3.972255
1.0	2.499458	1.850369	4.287728
1.5	1.766585	1.318857	2.692763
2.0	1.624994	1.143788	1.938106
2.5	1.783232	1.331824	2.240153
3.0	1.822619	1.217562	2.377118

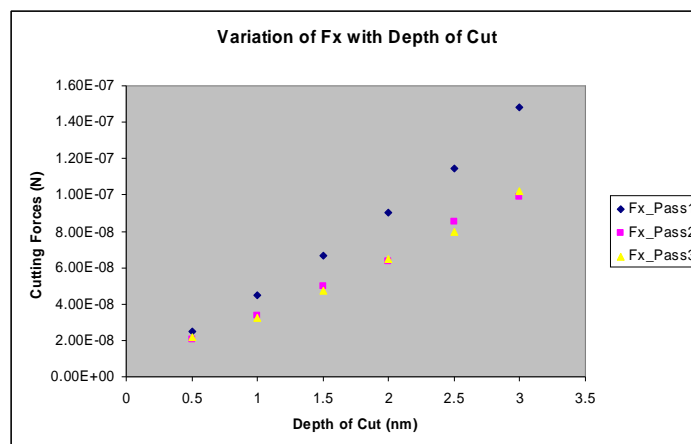


**Figure 6: Variation of  $F_x$  with Depth of Cut**

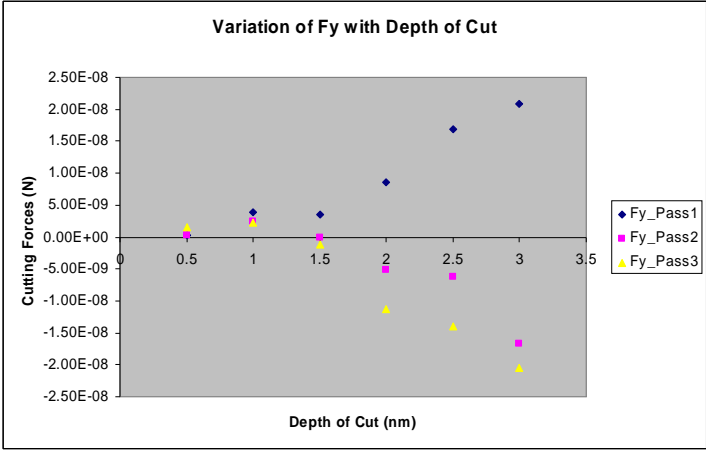


Figure 7: Variation of  $F_y$  with Depth of Cut

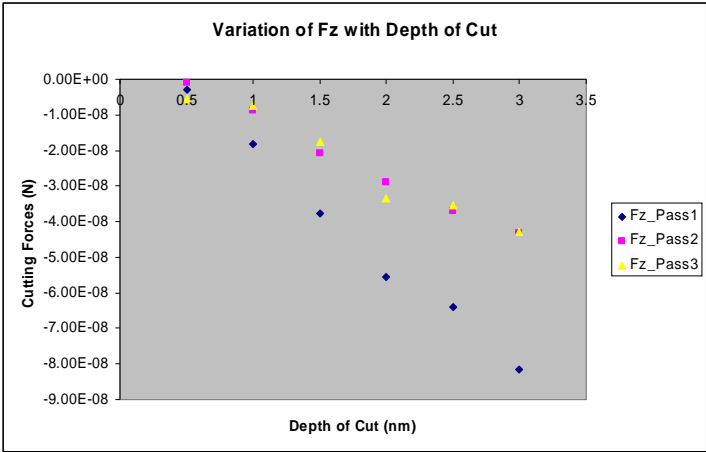


Figure 8: Variation of  $F_z$  with Depth of Cut

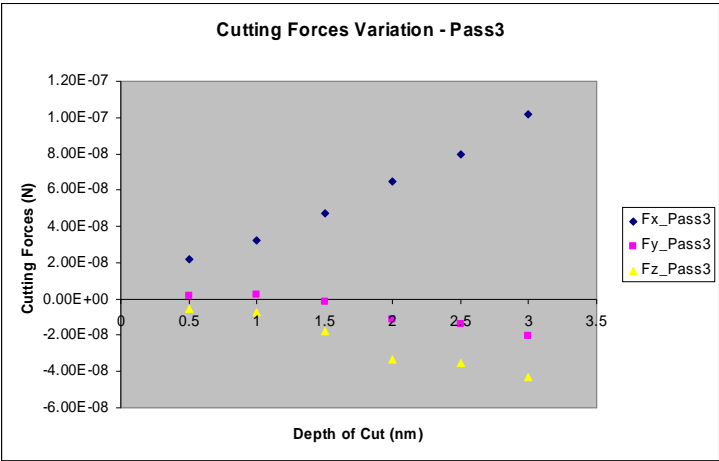
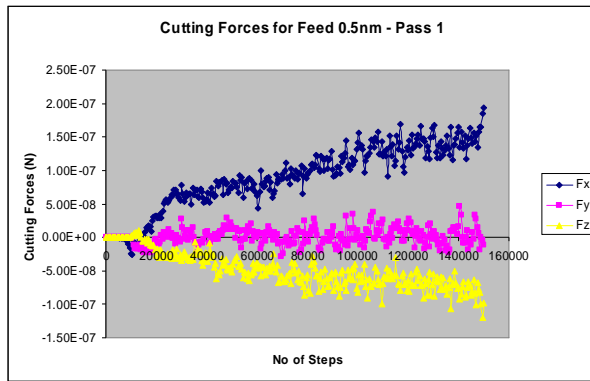


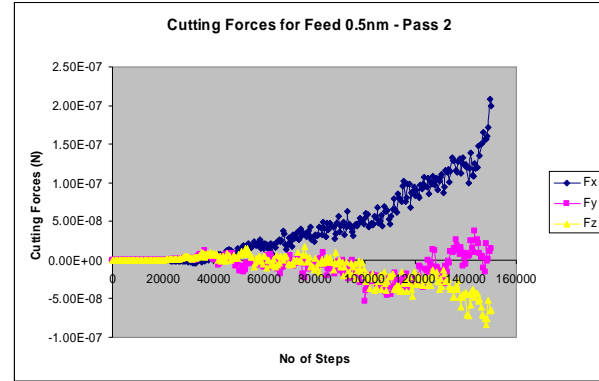
Figure 9: Variation of  $F_x$ ,  $F_y$  and  $F_z$  in Pass 3 with Depth of Cut

Table 4. Simulations for Different Feed (0.5 ~ 1.5nm), Depth of Cut =2nm, Cutting Speed = 150m/s, Rake Angle = 0°

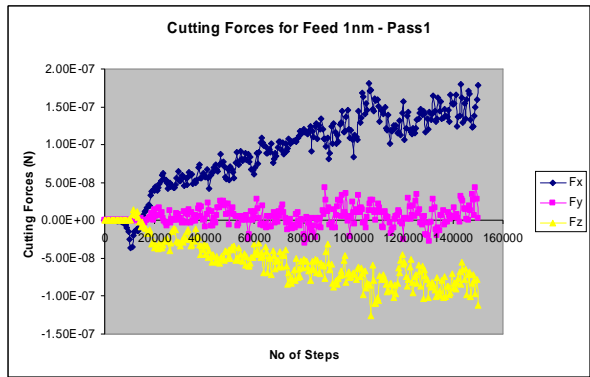
Feed (nm)	Pass 1	Pass 2	Pass 3
0.5			
1.0			
1.5			



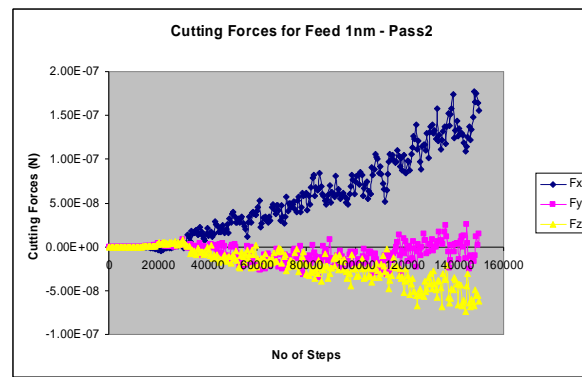
(a)



(b)

**Figure 10: Cutting Forces for Feed – 0.5nm (a - Pass 1 and b – Pass 2)**

(a)



(b)

**Figure 11: Cutting Forces for Feed – 1.0nm (a - Pass 1 and b – Pass 2)**

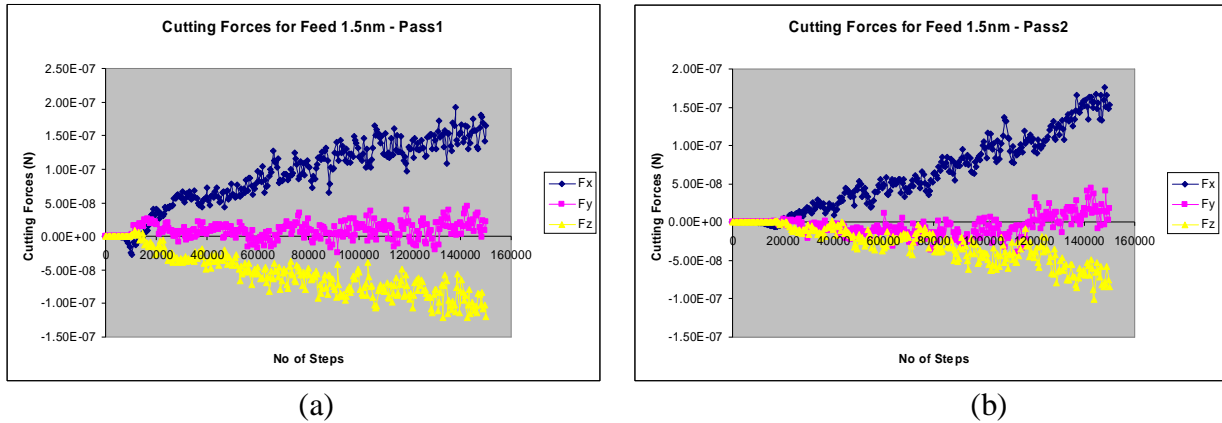


Figure 12: Cutting Forces for Feed – 1.5nm (a - Pass 1 and b – Pass 2)

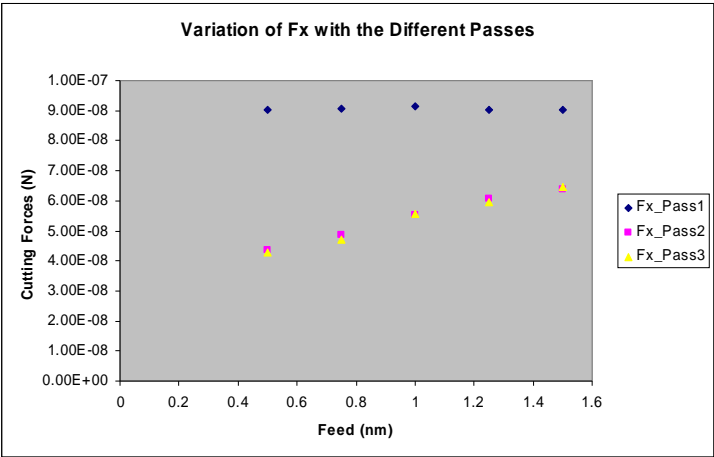
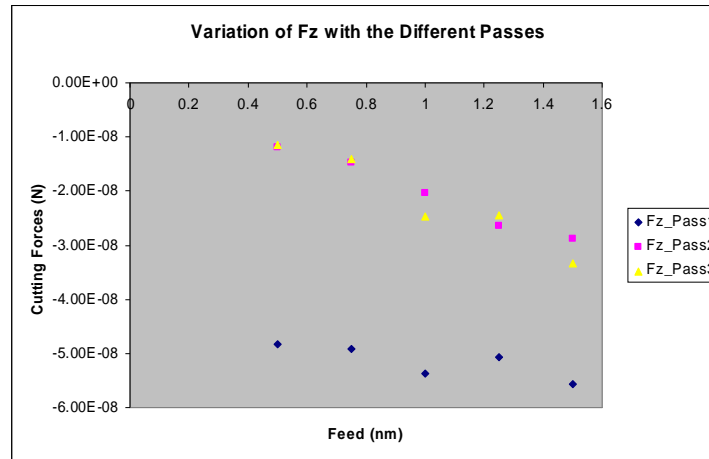


Figure 13: Variation of  $F_x$  with Passes 1~3



**Figure 14: Variation of  $F_z$  with Passes 1~3**

**Table 5: Force Ratios for Feed (0.5~1.5nm)**

Feed (nm)	$F_x/F_z$ Pass 1	$F_x/F_z$ Pass 2	$F_x/F_z$ Pass 3
0.5	1.868251	3.653598	3.699110
0.75	1.844857	3.325482	3.335340
1.0	1.700451	2.718395	2.246027
1.25	1.784327	2.289285	2.439838
1.5	1.624994	2.205282	1.938106

